Journal of Cellular Biochemistry 61:292–300 (1996)

Simultaneous Digital Imaging Analysis of Cytosolic Calcium and Morphological Change in Platelets Activated by Surface Contact

Masataka Ikeda, Hideo Ariyoshi, Jun-ichi Kambayashi, Masato Sakon, Tomio Kawasaki, and Morito Monden

Department of Surgery II, Osaka University Medical School, Suita, Osaka 565, Japan

Abstract The dynamic change of cytoplasmic Ca^{2+} concentration ($[Ca^{2+}]_i$) and morphological change were investigated simultaneously by confocal laser scanning microscopy using fluo-3 and by differential interference contrast optics in platelets activated by contact with the following types of surfaces: native glass and glass treated with poly-L-lysine (PLL), fibrinogen (Fg), or von Willebrand factor (vWF). The initial $[Ca^{2+}]_i$ values just after the surface contact were comparable (approximately 100 nM) among platelets deposited on the four surface types. On the PLL-surface, no morphological change or $[Ca^{2+}]_i$ elevation was observed. Glass-, Fg-, and vWF-surface adhered platelets showed pseudopod formation and spreading associated with the inhomogeneous $[Ca^{2+}]_i$ rise. The platelets on the Fg-surface were the most active in terms of $[Ca^{2+}]_i$ rise and morphological change. During pseudopod formation, the mean $[Ca^{2+}]_i$ value was maximal and localized high $[Ca^{2+}]_i$ zones were observed inside pseudopods, as well as in the center of the platelets. After spreading, high $[Ca^{2+}]_i$ zones still remained in the center of the cell. This new technique enabled simultaneous observation of $[Ca^{2+}]_i$ and cell shape and we clearly demonstrated a close relationship between $[Ca^{2+}]_i$ and morphological alterations.

Key words: platelets, morphological change, $[Ca^{2+}]_i$, confocal laser scanning microscopy, surface contact activation

One of the most important functions of platelets is to form hemostatic plug at the site of hemorrhage for maintaining vascular integrity. Platelets initially adhere to the subendothelial matrix exposed by vascular injury through interactions with collagen and vWF [Siess, 1989]. The adhesion of platelets is followed by shape change, aggregation, and secretion. An increase in the cytoplasmic Ca^{2+} concentration ($[Ca^{2+}]_i$) has been believed to play a major role in these responses [Siess, 1989; Kroll et al., 1991]. Although the morphological changes of platelets activated on subendothelial matrix or artificial surface has been well documented and fully characterized [Allen et al., 1979; Goodman et al., 1989], the precise intracellular relationship between the $[Ca^{2+}]_i$ rise and morphological changes is poorly understood.

Recent advances in digital imaging technique [Moore et al., 1990] and the introduction of the fluorescent Ca^{2+} indicator fura-2 [Grynkiewicz et al., 1985] have enabled us to gain further insight into the Ca^{2+} equilibrium temporally and spatially in a single platelet [Tsunoda et al., 1988; Nishio et al., 1992]. Heterogeneous $[Ca^{2+}]_i$ distribution was demonstrated in fura-2-loaded resting platelets [Tsunoda et al., 1988; Nishio et al., 1992; Ariyoshi and Salzman, 1995]. However, in platelets, previous observations could not be applied to study the dynamic correlation between $[Ca^{2+}]_i$ gradients and morphological changes during platelet activation, partly because of the small size of the platelets and possible artifacts due to immobilization [Waples et al., 1992; Okano et al., 1993]. The development of confocal laser scanning microscopy (CLSM) [Brakenhoff et al., 1989] and the new Ca^{2+}-sensitive dye fluo-3 [Minta et al., 1989] have allowed us to observe the $[Ca^{2+}]_i$ gradient in individual platelets with higher temporal and spatial resolution [Burnier et al., 1994; Nakato et al., 1992]. In this study, we investigated the relationship between the dynamic changes of $[Ca^{2+}]_i$ and the cell morphology in platelets exposed on physiological or artificial surfaces.

Received August 31, 1995; accepted October 26, 1995.

Address reprint requests to Dr. Hideo Ariyoshi, Department of Surgery II, Osaka University Medical School, 2-2 Yamadaoka, Suita, Osaka 565, Japan.

Since von Willebrand factor (vWF) and fibrinogen (Fg) are known to have crucial roles in platelet activation through ligand binding, we employed glass coverslips with surfaces covered with Fg or with vWF. A poly-L-lysine (PLL) was employed as the most quiescent surface, because it has been reported to allow platelet agglutination, but not to induce aggregation [Ariyoshi and Salzman, 1995].

MATERIALS AND METHODS

Materials

Fluo-3 acetoxymethyl ester (AM) was obtained from Molecular Probes (Eugene, OR, USA) and digitonin from Wako Chemicals (Osaka, Japan). PLL and Fg were purchased from Sigma (St. Louis, MO). Purified human vWF was kindly donated by Dr. Fujimura (Department of Blood Transfusion, Nara Medical College, Japan). Other chemicals were of the highest analytical grade available.

Platelet Preparation

Venous blood from healthy human volunteers was collected in plastic syringes through a 19-gauge needle containing one-tenth volume of 3.8% (w/v) sodium citrate. The first 2 ml of blood were discarded to prevent the contamination of tissue factor. Platelet rich plasma was prepared by centrifugation at 150*g* for 15 min at room temperature, and the platelets were loaded with fluo-3 by incubation with fluo-3/AM (10 μM) for 20 min at 37°C and for an additional 20 min at room temperature. The platelet concentration was adjusted to 3×10^8/ml.

Platelet Deposition and Activation

A thin glass coverslip equipped in the bottom of a Flexiperm chamber (Haraeus Biotechnologie, Hanau, Germany) was cleaned with ethanol and coating was carried out by contact with the solution of PLL, Fg, or vWF (0.2 mg/ml) for 1 h at room temperature, followed by evaporation. Fluo-3-loaded platelet suspension was diluted by 15 times in a modified Hepes–Tyrode buffer (129 mM NaCl, 8.9 mM $NaHCO_3$, 0.8 mM KH_2PO_4, 0.8 mM $MgCl_2$, 5.6 mM dextrose, and 10 mM Hepes, pH 7.4) and platelets were allowed to settle on the coverslips for 2 min at room temperature. After unattached platelets were removed by rapid rinsing with 0.4 ml of a modified Hepes–Tyrode buffer, 0.4 ml of the same buffer containing 1 mM $CaCl_2$ was added. The chamber was mounted on a Zeiss Axiovert 135 inverted microscope at room temperature, and the image scanning was started in 2 min after mounting.

Digital Imaging Microscopy

Digital imaging was carried out as described previously [Burnier et al., 1994] with some modifications. A CLSM equipped with an argon–ion laser (Carl Zeiss Microscope Systems LSM 410, Germany) was employed in this study. A 488 nm laser light was used for excitation; emitted light was collected through a FT510 dichroic beam splitter and finally passed through a 515-nm-long pass filter. A 63× oil-immersion objective (Plan-apochromat, numerical aperture = 1.4) was used, affording total magnification of 630×. For the detection of morphological changes of an individual platelet, laser light transmitted through the specimen was collected by differential interference contrast (DIC) optics. As the focal depth of the optical section can be controlled by the varying the size of the aperture pinhole in the emission pathway, we adjusted the size of the aperture pinhole to obtain the focal depth approximately 0.5 μm, which is sufficiently small to obtain the fluorescence intensity independently of the thickness of the specimen. Unequal distribution of the dye was negligible because the digitonin-treated (15–20 μM) and ionomycin treated (4 μM) platelets showed homogeneous fluorescence (data not shown). Artifacts due to photobleaching during temporal examination were minimal, since more than 96.5% of the initial fluorescence in each preparation was found to remain after 15-min laser exposure. We focused on the focal plane just above the glass coverslip to observe $[Ca^{2+}]_i$ change as a representative, because $[Ca^{2+}]_i$ changes of other focal planes with using z-sectioning were identical to that just above the glass coverslip (data not shown). Sixteen images acquired with a photo multiplier tube (PMT) detector were line-averaged in real time to reduce noise, and the average was digitized to 256 gray levels with an analog-to-digital converter. Images of 512 × 512 pixels were employed.

Determination of $[Ca^{2+}]_i$

Calibration of $[Ca^{2+}]_i$ was carried out by the method described by Gillo et al. [1993]. Briefly, 15–20 μM digitonin was added to quiescent platelets on a PLL-coated coverslip to obtain maximal fluorescence (Fmax), followed by the addi-

tion of 10 mM EGTA to obtain minimal fluorescence (Fmin). We calculated the $[Ca^{2+}]_i$ value from the fluorescent intensity (F) obtained with the Fmax and Fmin values, using the equation $[Ca^{2+}]_i = Kd \times (F\text{-}Fmin)/(Fmax\text{-}F)$. Kd is the dissociation constant for Ca^{2+}-bound fluo-3 that equals 320 nM, as indicated by Molecular Probes.

Calculations and Statistics

Results are expressed as the mean ±SEM. Comparisons between groups were performed using analysis of variance. A P-value of < 0.05 was considered significant.

RESULTS

Baseline $[Ca^{2+}]_i$ Images

Before morphological changes, the spatial distribution of $[Ca^{2+}]_i$ in platelets was inhomogeneous on all four types of surfaces. Localized hot spots were occasionally observed in the central zone of the cells (Fig. 1-(i) cell-d, Fig. 2-(i) cell-c, Fig. 3,4-(i) cell-d). There were no significant differences in the mean baseline $[Ca^{2+}]_i$ values; the initial values just after the surface contact, of platelets deposited on the PLL-, glass-, Fg-, and vWF-surface (Table I).

$[Ca^{2+}]_i$ Images and Morphological Changes in the Platelets Deposited on Four Types of Surfaces

After adhesion to the PLL-surface, most platelets showed neither pseudopod formation nor spreading. Only spherical enlargement was observed as shown in Figure 1-(i), and the spatial distribution of $[Ca^{2+}]_i$ became homogeneous throughout the spherical cell. During the period of enlargement of the platelets, no marked $[Ca^{2+}]_i$ change was observed (Fig. 1-(ii)). The mean $[Ca^{2+}]_i$ for the spherical platelets was 104.0 ± 8.5 nM (n = 12) and it was not significantly different from the base line $[Ca^{2+}]_i$ value (Table I).

The shape of most platelets deposited on the glass-, Fg-, or vWF-surface changed from discoid to pseudopod formation or spreading. The peak $[Ca^{2+}]_i$ value was obtained at the time of pseudopod formation and it was sometimes accompanied by $[Ca^{2+}]_i$ oscillation (Figs. 2–4-(ii)). $[Ca^{2+}]_i$ rise was not observed in the platelets that showed no marked shape change. High $[Ca^{2+}]_i$ zones were observed in the central zone or in the peripheral zone just beneath the plasma membrane (Fig. 2-(i) cell-a,b, Fig. 3-(i) cell-b, Fig. 4-(i) cell-a,b) and around pseudopod formation (Fig. 2-(i) cell-b, Fig. 3-(i) cell-a,c, Fig. 4-(i) cell-b). The peak $[Ca^{2+}]_i$ value at the time of pseudopod formation was followed by gradual decline as the platelet changed shape to spreading (Figs. 2–4-(ii)). The mean increase of $[Ca^{2+}]_i$ for the platelet on the Fg-surface was significantly higher than that for those on the native glass and vWF-surface, and the mean $[Ca^{2+}]_i$ values for the latter two surfaces were not significantly different. After spreading, the high $[Ca^{2+}]_i$ zones were observed solely in the center of the platelets, which was revealed to be the granulomere on the DIC images (Fig. 2-(i) cell-a, Fig. 3-(i) cell-a,c, Fig. 4-(i) cell-c). The distribution of $[Ca^{2+}]_i$ was homogeneous in the peripheral zone of the spread platelets (Fig. 2-(i) cell-a. Fig. 3-(i) cell-a).

DISCUSSION

The platelets deposited on the PLL-surface presented neither apparent shape change nor $[Ca^{2+}]_i$ rise, while those deposited on the other three surfaces formed pseudopods and spread with inhomogeneous $[Ca^{2+}]_i$ rise, consistent with the observations of Waples et al. [1992] and Okano et al. [1993], who reported $[Ca^{2+}]_i$ rise during morphological changes in contact-activated platelets. They suggested that the $[Ca^{2+}]_i$ rise is an initial signal of surface-induced platelet activation and subsequent morphological changes, but they were unable to present tempo-

Fig. 1. **i:** Spatial changes of $[Ca^{2+}]_i$ and the morphological changes in human platelets deposited on a Poly-L-lysine (PLL)-surface. **ii:** Temporal changes of mean $[Ca^{2+}]_i$ value in human platelets deposited on a PLL-surface. Fluo-3 loaded human platelets were prepared by incubating cells with 10 μM fluo-3/AM at 37°C for 20 min. After a 20-min incubation at room temperature, the platelets were deposited on a PLL-surface for 2 min. After unattached platelets were removed by rapid washing with a modified Hepes–Tyrode buffer, the same buffer containing 1 mM $CaCl_2$ was added. The chamber was mounted on a Zeiss inverted microscope and recording every 30 s was started 2 min after mounting. In panel (i), the spatial distribution of $[Ca^{2+}]_i$ (top row) and DIC images (the bottom row) at 0.5 (A), 3 (B), 7.5 (C), and 13 (D) min after the deposition are shown. **ii:** Typical temporal changes of mean $[Ca^{2+}]_i$ value of three cells (a, b, and c) are shown. *Arrows* with letters indicate the times at which the images were obtained. The characters on lines indicate the times at which shape changes of the three cells were observed with abbreviations as follows: Ad, adhesion to the coverslip; P, pseudopod formation; R, spherical change. Typical field from at least 3 independent experiments and the temporal changes of mean $[Ca^{2+}]_i$ in typical cells from the field are shown in i and ii, respectively. Bar = 5 μm.

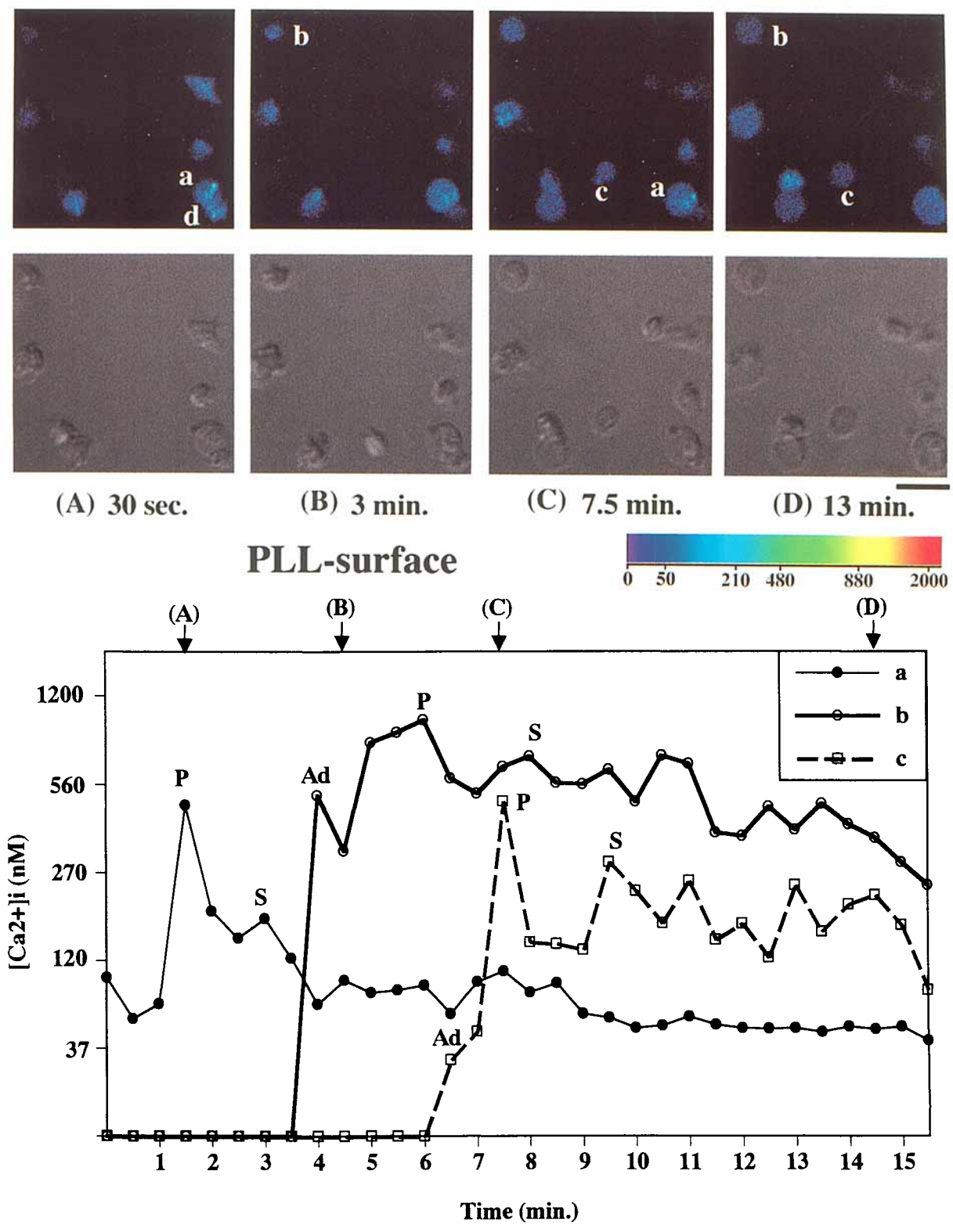
a
d
b
c
a
b
c
(A) 30 sec.
(B) 3 min.
(C) 7.5 min.
(D) 13 min.
PLL-surface
0 50 210 480 880 2000
(A)
(B)
(C)
(D)
a
b
c
P
Ad
S
[Ca2+]i (nM)
1200
560
270
120
37
1 2 3 4 5 6 7 8 9 10 11 12 13 14 15
Time (min.)

Figure 1.

TABLE I. Comparison of the Baseline and Peak $[Ca^{2+}]_i$ Values on the PLL-, Glass-, Fg-, or vWF-Surface*

$[Ca^{2+}]_i$ (nM)	PLL	n	Glass	n	Fg	n	vWF	n
Baseline	104.9 ± 7.7	13	81.6 ± 5.2	22	94.0 ± 8.7	37	101.3 ± 8.6	28
Peak	104.0 ± 8.5	12	398.9 ± 60.9**	14	766.5 ± 155.2†	13	419.4 ± 50.0‡	21

*There were no significant differences in baseline $[Ca^{2+}]_i$ values.
**$P = 0.02$ compared to PLL.
†$P < 0.0001$, $P = 0.004$, and $P = 0.003$ compared to PLL, glass, and vWF, respectively.
‡$P = 0.008$ compared to PLL (ANOVA).

ral and spatial analysis of $[Ca^{2+}]_i$, partly because of the insufficient temporal and spatial resolution of the system due to the limitation of fura-2 ratioing technique. In this study, we employed a confocal laser scanning system combined with fluo-3, which is a visible light-excitable dye that is brighter and more stable than fura-2, with which we were able to observe simultaneously the $[Ca^{2+}]_i$ and the morphological changes of contact activated platelets with superior temporal and spatial resolution. Our results suggest that the $[Ca^{2+}]_i$ rise is an initial signal in surface-induced platelet activation and in the subsequent morphological change. As the adherence to PLL, a high-molecular-weight cationic compound, was mainly due to the negative charge of the platelet plasma membrane [Salzman, 1971], it served as a quiescent surface on which no morphological change or $[Ca^{2+}]_i$ rise was induced.

In order to clarify the mode of surface activation of the platelets, we tested Fg- or vWF-surface, because these two proteins are major proteins involved in the platelet adhesion and aggregation [Siess, 1989]. On both surfaces, platelets formed pseudopods and spread as on the native glass. The platelet activation on Fg- or vWF-surface activation was probably mediated by glycoproteins IIb/IIIa (GpIIb/IIIa) or glycoproteins Ib (GpIb), respectively, because GpIIb/IIIa functions as the platelet receptor for Fg, and GpIb functions as the platelet receptor for vWF [Siess, 1989]. GpIIb/IIIa are linked to the underlying cytoskeleton and are believed to play a central role in shape change [Goodman et al., 1989] and Ca^{2+} transport across the plasma membrane [Brass, 1985; Powling and Hardisty, 1985]. $[Ca^{2+}]_i$ rise is also observed when GpIb binds to vWF [Kroll et al., 1991]. In the case of high shear stress induced platelet activation, vWF was reported to play a major role through the interaction with GpIb and GpIIb/IIIa [Ikeda, 1991]. The probability of further absorption of plasma proteins was negligible because each surface was saturated with Fg or vWF, and the same morphological change was observed when washed platelets were deposited (data not shown). The effects of thrombin or ADP secreted from other activated platelets were also minimal, because a similar pattern of morphological change was observed in the presence of heparin (1 U/ml), a catalytic cofactor for antithrombin III or apyrase (0.1 mg/ml), an ADP scavenger (data not shown). The baseline $[Ca^{2+}]_i$ values on these three surfaces did not differ, but the peak $[Ca^{2+}]_i$ on the Fg-surface was significantly higher than that on the either native glass or vWF-surface and was correlated with morphological change; 90.8% (119/131) of the platelets showed spreading 20 min after the deposition on a Fg-surface, compared to 73.6% (64/87) and 48.6% (85/175) of the platelets on the glass- and vWF-surface, respectively. These observations may suggest the existence of signal transduction system stimulated by the binding of vWF or Fg with GpIb or GpIIb/IIIa that causes a $[Ca^{2+}]_i$ rise integral to morphological change. The more marked rise of $[Ca^{2+}]_i$ in Fg-adherent platelets may suggest the central role of GpIIb/IIIa in regulating $[Ca^{2+}]_i$ during surface activation.

$[Ca^{2+}]_i$ plays a key role in platelet morphological change and platelet shape change is mainly regulated by the activation of myosin light chain kinase (MLCK), a Ca^{2+}-calmodulin-dependent kinase [Daniel et al., 1984]. Phosphorylation of myosin light chain by MLCK leads to drastic reorganization of cytoskeletal structure [Siess, 1989]. When ionomycin is the stimulus, half-maximal myosin phosphorylation occurs at the $[Ca^{2+}]_i$ level of 600 nM, and no shape change is observed at the $[Ca^{2+}]_i$ level of 300 nM [Rink et al., 1982; Hallam et al., 1985]. However shape change was observed even on both glass- and vWF-surfaces on which the platelets showed elevation of $[Ca^{2+}]_i$ to 398.9 ± 60.9 nM and

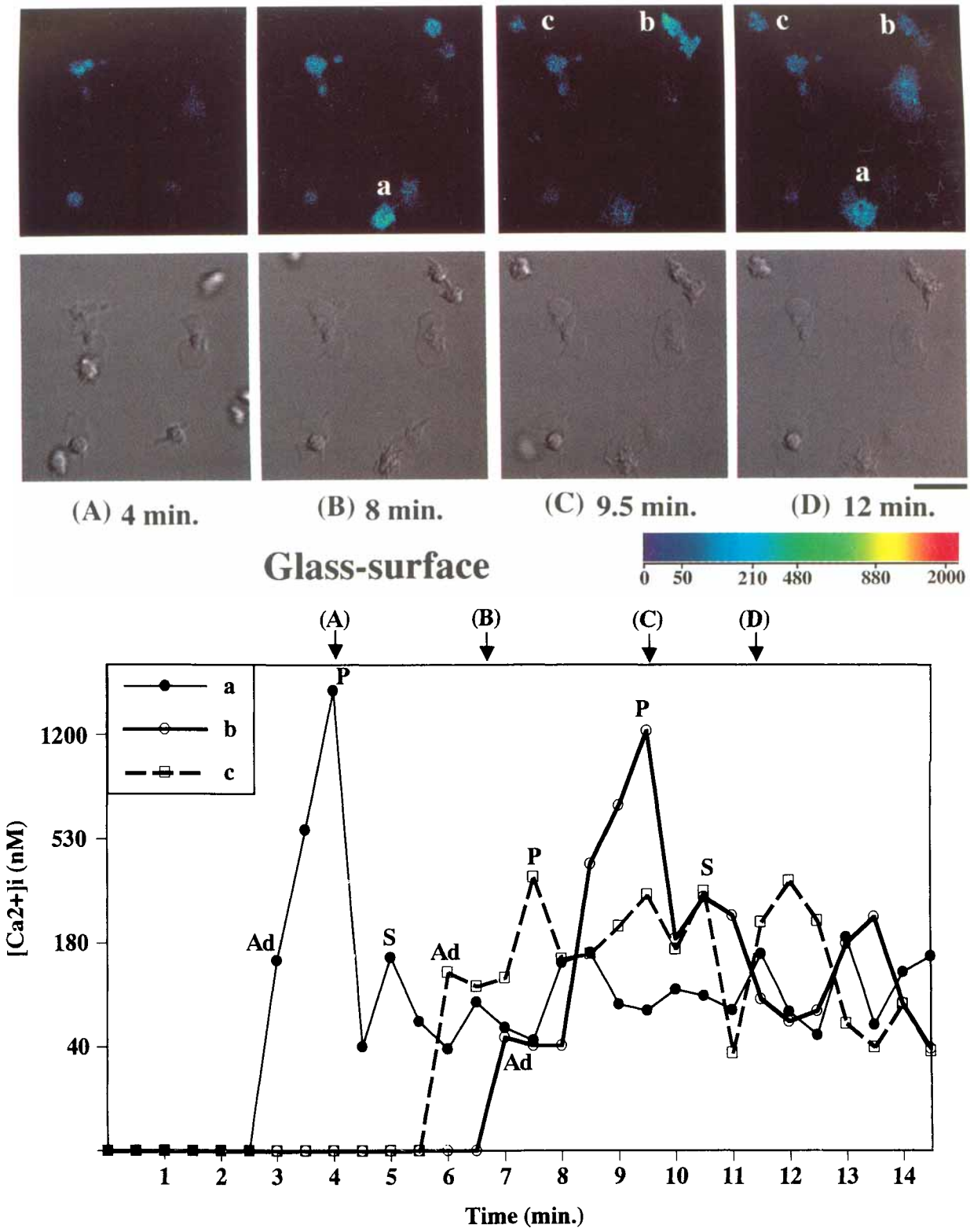

Fig. 2. **i:** Spatial changes of $[Ca^{2+}]_i$ and the morphological changes in human platelets deposited on native glass. **ii:** Temporal changes of mean $[Ca^{2+}]_i$ value in human platelets deposited on a glass-surface. **i:** Spatial distribution of $[Ca^{2+}]_i$ (top row) and DIC images (bottom row) at 4 (A), 8 (B), 9.5 (C), and 12 (D) min after the deposition are shown. The characters on lines indicate the times at which shape changes of the three cells were observed with abbreviations as follows: Ad, adhesion to the coverslip; P, pseudopod formation; S, spreading. For further detail, see the legend for Fig. 1.

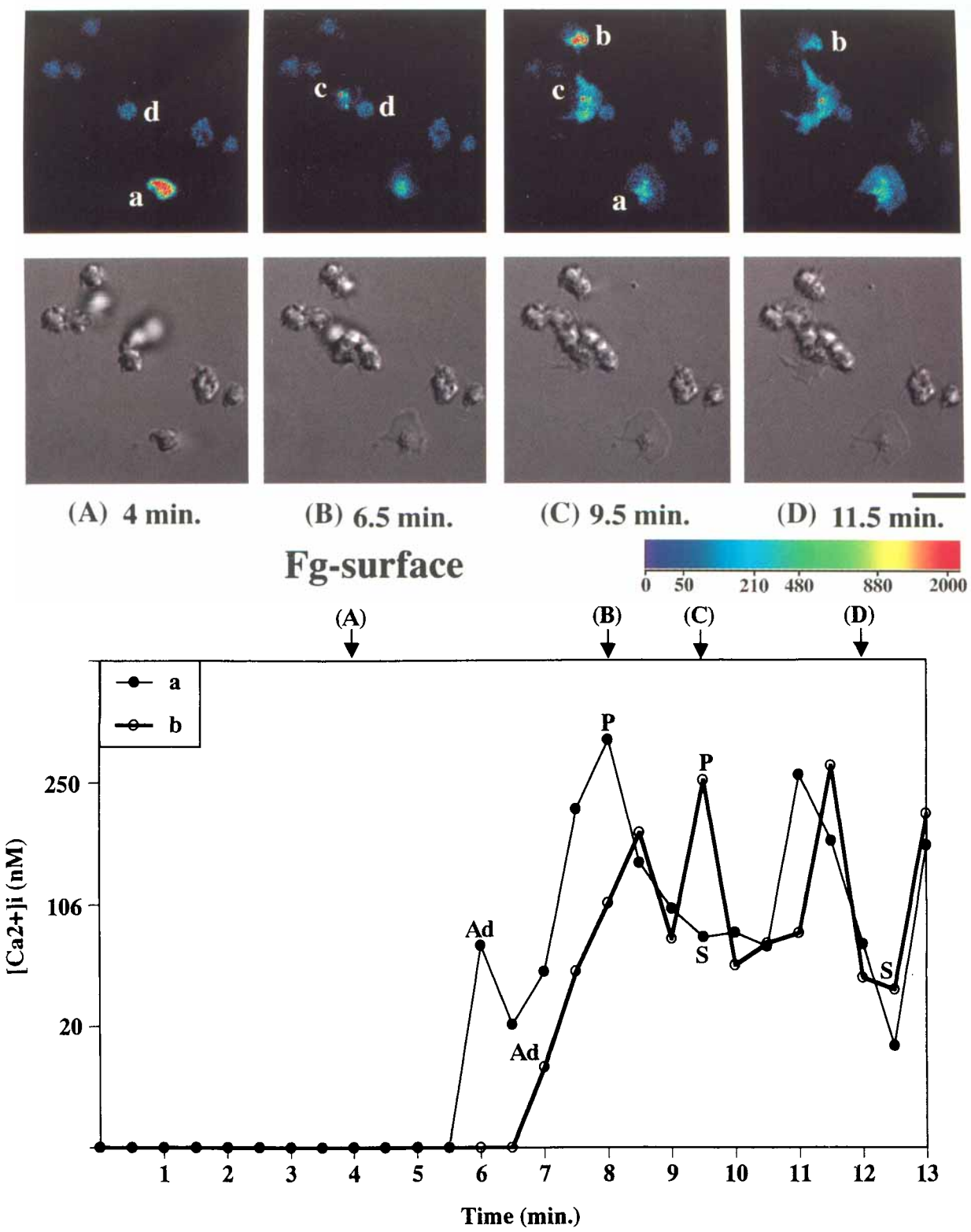

Fig. 3. **i:** Spatial changes of $[Ca^{2+}]_i$ and the morphological changes in human platelets deposited on a Fg-surface. **ii:** Temporal changes of mean $[Ca^{2+}]_i$ value in human platelets deposited on a Fg-surface. **i:** Spatial distribution of $[Ca^{2+}]_i$ (top row) and DIC images (bottom row) at 4 (A), 6.5 (B), 9.5 (C), and 11.5 (D) min after the deposition are shown. Characters on lines indicate the times at which shape changes of the three cells were observed with abbreviations as follows: Ad, adhesion to the coverslip; P, pseudopod formation; S, spreading. For further detail, see the legend for Fig. 1.

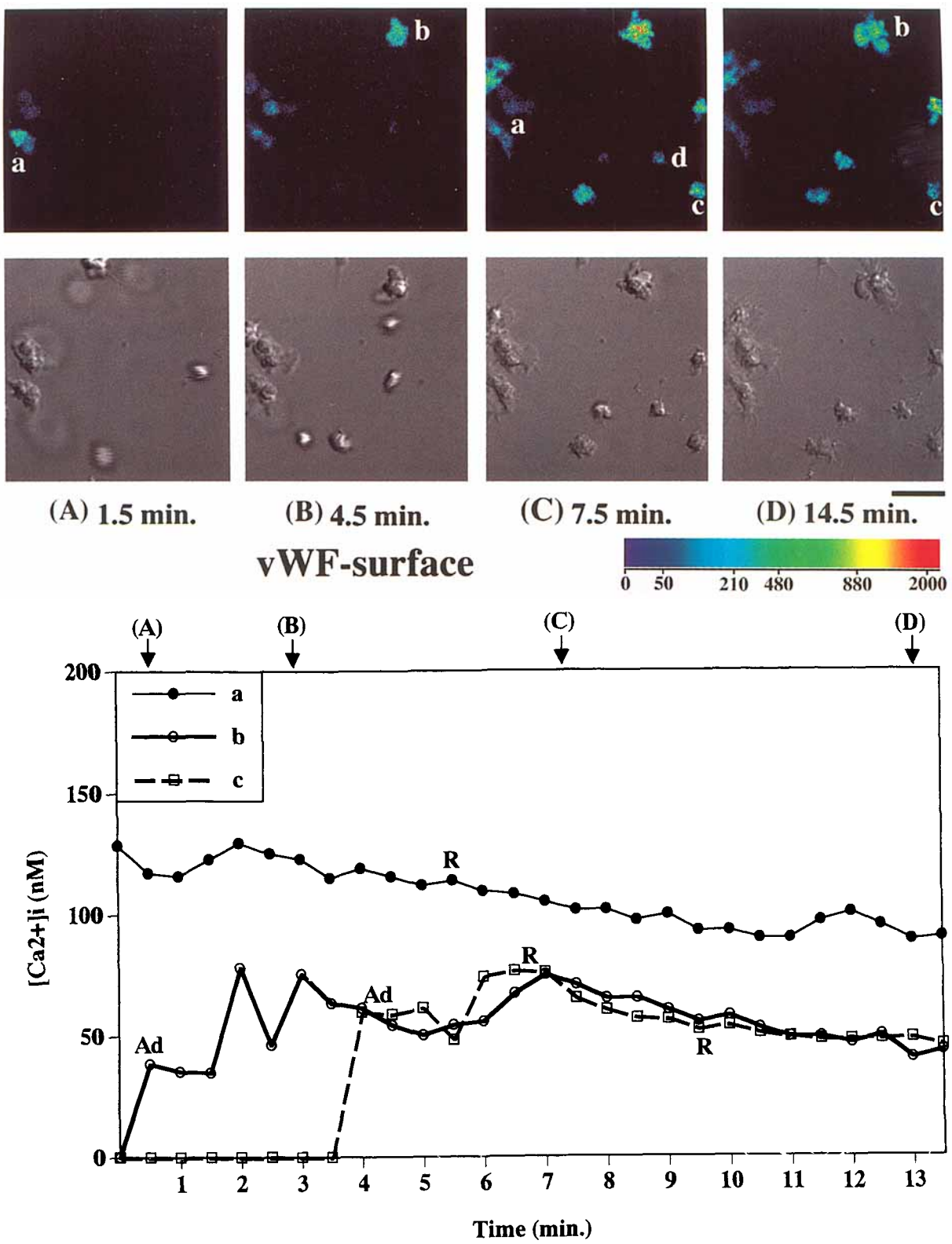

Fig. 4. **i:** Spatial changes of $[Ca^{2+}]_i$ and the morphological changes in human platelets deposited on a vWF-surface. **ii:** Temporal changes of mean $[Ca^{2+}]_i$ value in human platelets deposited on a vWF-surface. **i:** Spatial distribution of $[Ca^{2+}]_i$ (top row) and DIC images (bottom row) at 1.5 (A), 4.5 (B), 7.5 (C), and 14.5 (D) min after the deposition are shown. The characters on lines indicate the times at which shape changes of the three cells were observed with abbreviations as follows: Ad, adhesion to the coverslip; P, pseudopod formation; S, spreading. For further detail, see the legend for Fig. 1.

419.4 ± 50.0 nM, respectively. This discrepancy may be explained by the existence of a local $[Ca^{2+}]_i$ rise. Local high $[Ca^{2+}]_i$ values exceeding 600 nM were observed inside the pseudopods and in the peripheral zone just beneath the plasma membrane. It is likely that myosin phosphorylation may therefore take place at the loci of marked local $[Ca^{2+}]_i$ elevation. In well-spread platelets, high $[Ca^{2+}]_i$ zones were observed mainly in the hillock of the granulomere that was confirmed by DIC microscopy [Allen et al., 1979]. Because the morphological alterations were apparently completed at this point, it is unlikely that the observed centralized $[Ca^{2+}]_i$ rise plays any role in platelet morphological change. Since the hillock of the granulomere is related to exocytosis of dense bodies [Allen et al., 1979], central $[Ca^{2+}]_i$ rise may be related to platelet release reaction.

In conclusion, we observed the platelet $[Ca^{2+}]_i$ and its morphological change simultaneously by employing CLSM and DIC optics using the Ca^{2+} indicator, fluo-3. The results clearly demonstrated that both temporal $[Ca^{2+}]_i$ and local $[Ca^{2+}]_i$ gradients were well correlated with platelet shape change induced by contact activation. The possible roles of localized $[Ca^{2+}]_i$ rise controlling cell shape was suggested. We anticipate that this technique will provide further insight into the dynamic $[Ca^{2+}]_i$ regulation related to platelet adhesion and aggregation upon vascular injury.

ACKNOWLEDGMENTS

The authors wish to thank Dr. Y. Fujimura for the kind donation of human purified vWF.

REFERENCES

Allen RD, Zacharski LR, Widirstky ST, Rosenstein R, Zaitlin LM, Burgess DR (1979): Transformation and motility of human platelets. Details of the shape change and release reaction observed by optical and electron microscopy. J Cell Biol 83:126–142.

Ariyoshi H, Salzman EW (1995): Spatial distribution and temporal change in cytosolic pH and $[Ca^{2+}]$ in resting and activated single human platelets. Cell Calcium 17:317–326.

Brakenhoff GJ, Van Spronsen EA, Van der Voort HTM, Nanninga N (1989): Three-dimensional confocal fluorescence microscopy. Methods Cell Biol 30:379–398.

Brass LF (1985): Ca^{2+} transport across the platelet plasma membrane. J Biol Chem 260:2231–2236.

Burnier M, Centeno G, Burki E, Brunner HR (1994): Confocal microscopy to analyze cytosolic and nuclear calcium in cultured vascular cells. Am J Physiol 266:C1118–C1127.

Daniel JL, Molish IR, Rigmaiden M, Stewart G (1984): Evidence for a role of myosin phosphorylation in the initiation of the platelet shape change response. J Biol Chem 259:9826–9831.

Gillo B, Ma Y-S, Marks AR (1993): Calcium influx in induced differentiation of murine erythroleukemia cells. Blood 81:783–792.

Goodman SL, Grasel TG, Cooper SL, Albrecht RM (1989): Platelet shape change and cytoskeletal reorganization on polyurethaneureas. J Biomed Mater Res 23:105–123.

Grynkiewicz G, Poenie M, Tsien RY (1985): A New Generation of Ca^{2+} indicators with greatly improved fluorescence properties. J Biol Chem 260:3440–3450.

Hallam TJ, Daniel JL, Kendrick-Jones J, Rink TJ (1985): Relationship between cytoplasmic free calcium and myosin light chain phosphorylation in intact platelets. Biochem J 232:373–377.

Ikeda Y, Handa M, Kawano K, Kamata T, Murata M, Araki Y, Anbo H, Kawai Y, Watanabe K, Itagaki I, Sakai K, Ruggeri ZM (1991): The role of von Willebrand factor and fibrinogen in platelet aggregation under varying shear stress. J Clin Invest 87:1234–1240.

Kroll MH, Harris TS, Moake JL, Handin RI, Schafer AI (1991): von Willebrand factor binding to platelet GpIb initiates signals for platelets activation. J Clin Invest 88:1568–1573.

Minta A, Kao JPY, Tsien RY (1989): Fluorescent indicators for cytosolic calcium based on rhodamine and fluorescein chromophores. J Biol Chem 264:8171–8178.

Moore EDW, Becker PL, Fogarty KE, Williams DA, Fay FS (1990): Ca^{2+} imaging in single living cells: theoretical and practical issues. Cell Calcium 11:157–179.

Nakato K, Furuno T, Inagaki K, Teshima R, Terao T, Nakanishi M (1992): Cytosolic and intranuclear calcium signals in rat basophilic leukemia cells as revealed by a confocal fluorescence microscope. Euro J Biochem 209: 745–749.

Nishio H, Ikegami Y, Nakata Y, Segawa T (1992): Fluorescence digital image analysis of thrombin and ADP induced rise in intracellular Ca^{2+} concentration of single blood platelets. Neurochem Int 21:75–81.

Okano T, Suzuki K, Yui N, Sakurai Y, Nakahama S (1993): Prevention of changes in platelet cytoplasmic free calcium levels by interaction with 2-hydroxyethyl methacrylate/styrene block copolymer surfaces. J Biomed Mater Res 27:1519–1525.

Powling MJ, Hardisty RM (1985): Glycoprotein IIb–IIIa complex and Ca^{2+} influx into stimulated platelet. Blood 66:731–734.

Rink TJ, Smith SW, Tsien RY (1982): Cytoplasmic free Ca^{2+} in human platelets: Ca^{2+} thresholds and Ca-independent activation for shape-change and secretion. FEBS Lett 148:21–26.

Salzman EW (1971): Role of platelets in blood-surface interactions. Fed Proc 30:1503–1508.

Siess W (1989): Molecular mechanisms of platelet activation. Physiol Rev 69:58–178.

Tsunoda Y, Matsuno K, Tashiro Y (1988): Spatial distribution and temporal change of cytoplasmic free calcium in human platelets. Biochem Biophys Res Commun 156: 1152–1159.

Waples LM, Olotundare OE, Goodman SL, Albrecht RM (1992): Changes in intracellular Ca^{2+} and structure in platelets contacting synthetic substrates. Cells Mater 2:299–308.